Simultaneous in-chamber MHz sensing of CO, H 2 O, temperature, and pressure via mid-infrared laser absorption in a rotating detonation rocket engine

Nicholas Kuenning, Anil Nair, Alex Keller, Nicolas Minesi, Raymond Spearrin, Ozen Emre, Kriesel Jason, Bennewitz John W., Burr Jason, Dancyzk Stephen A.

Simultaneous in-chamber MHz sensing of CO, H_2O, temperature, and pressure via mid-infrared laser absorption in a rotating detonation rocket engine

Nicholas M. Kuenning*, Anil P. Nair†, Alex R. Keller‡, Nicolas Q. Minesi §, and R. Mitchell Spearrin¶
University of California, Los Angeles (UCLA), Los Angeles, CA 90095, USA

Emre Ozen, Jason Kriesel
Opto-Knowledge Systems, Inc. (OKSI), Torrance, CA 90502, USA

Blaine Bigler‖
Jacobs Technology Inc., Edwards AFB, CA 93524, USA

John W. Bennewitz**
The University of Alabama in Huntsville, Hunstville, AL 35899, USA

Jason Burr†† and Stephen A. Dancyzk‡‡
AFRL/RQRC, Combustion Devices Branch, Air Force Research Laboratory, Edwards Air Force Base, CA 93524, USA

A mid-infrared laser absorption sensing strategy for simultaneous measurement of carbon monoxide (CO), water (H_2O), pressure, and temperature has been developed for in-chamber MHz rate measurements of gas dynamics in rotating detonating rocket engines (RDREs). Trapezoidal modulation via bias-tee circuitry integrated with two distributed feedback quantum cascade lasers provided sufficient scan depth to capture rovibrational transitions in the fundamental bands of CO and H_2O (at 5 µm) with a time resolution of 1 µs. The two lasers are multiplexed into a single InF_3 single-mode fiber for light delivery to the annulus of a methane-oxygen fueled RDRE at the Air Force Research Lab in Edwards, CA. This demonstration, utilizing a single detector, yields quantitative temperature, pressure, and two-species measurements at 1 MHz over a range of expected in-chamber post-detonation conditions, 1500–3000 K and 1–5 atm. The flow rate and equivalence ratios studied in this paper are relevant to the Air Force Research Laboratory's Modeling Validation for Propulsion (MVP) efforts.

*Ph.D. Student, Mechanical and Aerospace Engineering Department. AIAA Member
†Ph.D. Mechanical and Aerospace Engineering Department. AIAA Member
‡Ph.D. Student, Mechanical and Aerospace Engineering Department. AIAA Member
§Postdoctoral Scholar, Mechanical and Aerospace Engineering Department. AIAA Member
¶Associate Professor, Mechanical and Aerospace Engineering Department. AIAA Member
‖Research Engineer, Jacobs Technology Inc., 10 East Saturn Blvd., Edwards AFB, CA 93524. AIAA Member
**Assistant Professor, Department of Mechanical and Aerospace Engineering. AIAA Senior Member
††Research Scientist, AFRL/RQRC, 10 East Saturn Blvd., Edwards AFB, CA 93524. AIAA Member
‡‡Research Scientist, AFRL/RQRC, 10 East Saturn Blvd., Edwards AFB, CA 93524. AIAA Member

I. Introduction

Rotating detonation engines (RDREs) have been the focus of heightened research interest in recent years due to their theoretical thermodynamic benefits over deflagration-based combustion and their simple system architecture when compared to pulse-detonation engines [1]. The increased post-reaction pressures produced by the detonation wave allows a greater amount of work to be extracted from the combustion gas for the same input propellant mass. Unfortunately, the dynamic unsteady nature of detonations and extreme range of thermodynamic conditions covered across very short time scales (<millisecond) in detonation engines have made these systems challenging to control, model, and design [2], slowing technical maturity. For instance, the interaction between propellant injection and detonation-wave propagation is not well understood and could partly explain underperformance via mechanisms such as temporary flow reversal or parasitic deflagration [1, 2]. There exists a distinct need for quantitative in-chamber data for RDREs to understand the complex thermochemistry and combustion physics. Laser absorption spectroscopy (LAS) has proven a useful diagnostic method for quantitative temperature and species measurements in detonation environments. In recent years, the temporal bandwidth of LAS has increased to MHz rates, providing sufficient temporal resolution to resolve the intra-cycle transients of RDREs with 5–20 kHz cycle frequencies [3–10]. Here, we present a time-division multiplexed mid-infrared laser absorption sensing strategy capable of 1-MHz measurements of temperature and two major combustion species (CO and H_2O) at high-temperature and elevated-pressure detonation conditions. By measuring the major combustion products as well as the key thermodynamic parameters of temperature and in-chamber pressure, the combustion progress and dynamics can be evaluated in the detonation flowfield.

In section II we outline how the pressure, temperature and species number densities are extracted from LAS data. We then detail the experimental setup used to obtain the in-situ LAS measurements for the RDRE. Section III describes key steps in the data processing and provides both time-resolved and intra-cycle mean thermophysical properties for test cases relevant for AFRL's Modeling Validation for Propulsion (MVP) effort [11].

II. Methods

A. Laser Absorption Spectroscopy

The fundamental vibrational bands of CO and H_2O in the mid-infrared—centered near 4.7 μm and 6.3 μm, respectively—are orders of magnitude stronger than overtone and combination bands in the near-infrared and can provide high species sensitivity at short optical path-lengths (~1 cm) making them suitable for analyzing thermochemistry in the annuli of RDREs. The transitions measured for each targeted species were selected for their strength, temperature sensitivity, and relative spectral isolation from other combustion species at conditions representative of the downstream portion of an RDRE combustor (1000–4000 K and 1–5 atm). In this study we employ a scanned-wavelength direct absorption (scanned-DA) spectroscopic technique wherein we modulate the injection-current of each light source to scan the wavelength of the emitted laser light to capture the full lineshape of the transitions. Though slower than fixed-wavelength direct absorption (fixed-DA), spectrally scanned DA can provide additional information regarding line broadening and greater confidence in the baseline non-absorbing signals. This facilitates corrections of both beam steering and thermal emission as needed, which are significant issues in harsh environments for fixed-DA methods [12]. Spectrally scanned DA is also insensitive to line shifts due to collisional effects and potential laser drift during an experimental campaign.

For CO, the line cluster including the P(2,20) and P(0,31) transitions in the fundamental ($\Delta v = +1$) band was targeted, where P(v'',J'') indicates the respective lower vibrational (v'') and rotational (J'') quanta. The letter P indicates the transition belongs to the P-branch of the band correlating to a decrease in rotational number $J' = J'' - 1$. These two lines were selected for their temperature sensitivity, as described in previous works [9, 13, 14]. Notably, both transitions can be accessed within the tuning depth of a single narrow band light source tuned at 1 MHz. For H_2O, the $24_{0,24} \rightarrow 25_{1,25}$ and $24_{1,24} \rightarrow 25_{0,25}$ rovibrational doublet of the ν_2 fundamental band was targeted near 5.0 μm, where the notation $J_{K_a,\,K_b}$ refers to the rotational quantum number J and angular momentum K about the a and b axes. This line pair will be referred to as the "H_2O doublet" for the remainder of this work. This transition has minimal interference from other high-temperature combustion species and is located in the same spectral region as the targeted CO transitions, enabling the measurement of the two species on a single detector using one narrow spectral-bandpass filter, as detailed in II.B. This transition is measured along with the neighboring P(1,27) transition of CO, which provides additional spectral information for CO, leading to enhanced precision in the temperature, pressure, and CO density measurements.

The Beer-Lambert law, shown in Eq. 1, relates the measured attenuated light I_t to the thermophysical properties of

the flow: number density of species j, n_j [cm^{-3}], and temperature, T [K], as well as the path length L [cm].

$$\alpha_{ij}(\nu) = -\ln\left(\frac{I_t}{I_0}\right) = n_j L S_{ij}(T)\phi_{ij}(\nu, P, T, X_Y) \tag{1}$$

Each rovibrational transition has a temperature-dependent linestrength S_{ij} which is documented in databases such as HITEMP [15] and a lineshape function ϕ which depends on temperature, pressure, and gas composition. The gas composition X_Y, temperature, and pressure are not pre-determined at the beginning of the analysis so the absorbance α is integrated over the spectral domain, noting that $\int_{-\infty}^{\infty} \phi_{ij}(\nu)d\nu = 1$. The result is shown in Eq. 2 in which the integrated absorbance area of transition i of species j, A_{ij} [cm^{-1}], no longer depends on the lineshape function ϕ.

$$A_{ij} = \int_{-\infty}^{\infty} \alpha_{ij}(\nu)d\nu = n_j L S_{ij}(T) \tag{2}$$

With this integration, the absorbance area is dependent on n_j, T and linestrength. The following details a method of determining the pressure and temperature of the gas independently from the absolute magnitude of the absorbance areas.

Commonly in LAS, the temperature can be measured by using a ratio of transition areas [12, 16]. In a previous work [17], we developed a Boltzmann population fit method to account for more than two transitions to measure temperature and number density with reduced uncertainty. Equation 3 details how the ratio of integrated absorbance areas to the reference linestrength of transition i, $S^0_{i,\mathrm{CO}}$ [cm^{-1}/molecule·cm^{-2}], relates to n_{CO} and T, where E_i [cm^{-1}] is the lower-state energy of the transition [15], $T_0 = 296$ K and $hc/k = 1.44$ cm·K.

$$\ln\left(\frac{A_{i,\mathrm{CO}}}{S^0_{i,\mathrm{CO}}}\right) = \ln(L n_{\mathrm{CO}} q(T)) - \frac{hc}{k_{\mathrm{B}}}\left(\frac{1}{T} - \frac{1}{T_0}\right)E_i \tag{3}$$

$q(T)$ represents the partition function taken from HITRAN [18, 19] multiplied by a stimulated emission factor, see Eq. 4, where $\nu_0 = 2005$ cm^{-1} [17].

$$q(T) = \frac{Q(T_0)}{Q(T)}\frac{1 - \exp\left(-\frac{hc}{k_{\mathrm{B}}T}\nu_0\right)}{1 - \exp\left(-\frac{hc}{k_{\mathrm{B}}T_0}\nu_0\right)} \tag{4}$$

Writing Eq. 3 in the form of $Y = aE_i + b$ yields the slope and intercept, a and b, which are rearranged to solve for T and n_{CO} as shown in 5 and 6.

$$T = \frac{1}{1/T_0 - a k_{\mathrm{B}}/hc} \tag{5}$$

$$n_{\mathrm{CO}} = \frac{\exp(b)}{L q(T)} \tag{6}$$

By utilizing the Boltzmann population fit, T is determined independently from other thermophysical properties and is considered a known for the following steps.

Pressure, P [atm], is determined through Eq. 7 by using the measured collisional linewidth $\Delta\nu_C$ [cm^{-1}] and the calculated broadening coefficient $\gamma_{\mathrm{CO,mix}}$ [cm^{-1}/atm].

$$P = \frac{\Delta\nu_C}{2\gamma_{\mathrm{CO,mix}}(T, X_Y)} \tag{7}$$

The collisional linewidth is dependent on the number of collisions per second with the absorbing species, making it linearly dependent on pressure; however, species of different collisional diameters and masses can raise or lower this linewidth based on the gas composition. $\gamma_{\mathrm{CO,mix}}$ accounts for the difference in collision rate for different species by summing of collisional-broadening coefficients of all constituent species with CO, $\gamma_{\mathrm{CO},j}$, weighted by their mole fraction as shown in Eq. 8.

$$\gamma_{\mathrm{CO,mix}}(T, X_Y) = \sum_j X_j \gamma_{\mathrm{CO},j} \tag{8}$$

This calculation poses a challenge given limited documentation of reference broadening coefficients for many combustion species. Nair et at. [20] provides a method for simplifying this calculation by considering only combustion species with $X_j > 1\%$ and documents the necessary reference coefficients to calculate $\gamma_{\mathrm{CO,mix}}$ for CH_4–O_2 combustion. Uncertainty

remains regarding the composition of the gas as other major combustion species are not measured, thus the remaining species must be approximated using chemical models. Here, the GRI-MECH 3.0 [21] is paired with the CalTech Shock and Detonation Toolbox [22] in CANTERA [23] to approximate the gas composition immediately behind the detonation wave (frozen composition) and when chemically equilibrated after being isentropically expanded. These two conditions represent the extremes of flow composition for a given equivalence ratio ϕ. Evaluating $\gamma_{CO,mix}$ at the frozen and equilibrated conditions shows $< 5\%$ variation between the two conditions so the average can serve as a good approximation of the broadening coefficient, allowing P to be determined.

With temperature determined, n_{H_2O} [cm^{-3}] is found using Eq. 9.

$$n_{H_2O} = \frac{A_{H_2O}}{S_{H_2O}(T)L} \tag{9}$$

After finding the H_2O number density, the quantities of measured species, temperature and pressure have been fully determined. It should be noted that CO and H_2O typically account for more than half of the product gas composition for fuel-rich CH_4–O_2 combustion.

B. Experimental Setup

Two continuous-wave distributed-feedback (DFB) quantum cascade lasers (QCL) (ALPES Lasers), tunable from 2001 to 2012 cm^{-1}, are used as the narrow-band light sources for probing the CO and H_2O transitions identified in Section II.A. A bias-tee (SigaTek SB12D2D) configuration, detailed in [9] is used to bypass the bandwidth limitation of commercial off-the-shelf laser controllers used for this application (Arroyo 6300 series), extending the achievable scan rates of these lasers from 100s of kHz to several MHz. Trapezoidal waveforms optimized for maximizing scan depth are supplied directly by a function generator (Rigol DG1000Z) [24]. At 1 MHz, a scan depth of 0.9 cm^{-1} for the CO spectrum and a scan depth of 0.7 cm^{-1} for the H_2O spectrum can be achieved, enabling full resolution of the targeted spectral features even at elevated pressures.

The two QCL laser beams are combined using a 50/50 CaF_2 beamsplitter, and further time-division-multiplexed by utilizing square-wave injection current waveforms at a duty cycle of 45% from a single function generator that enables consistent phase-locking of the signals. This time-division-multiplexing across 1 µs can be seen in the top right of Fig. 1. Light from each laser is collected by a single photovoltaic (PV) detector (Vigo PVMI-4TE-8-1x1), with a measurement bandwidth of 196 MHz. The beam path outside of the engine annulus is constantly purged with nitrogen to avoid interference from recirculating combustion gas. The laser beam is pitched through a 0.5-in diameter sapphire window and reflected off of a polished flat at a half angle of $\sim 5°$. The RDRE annulus width and window recess provide a total optical path length L of 1.30 cm with the retro-reflection. The measurement location is 2.25 in from the injector face, providing measurements at higher pressures compared to previous works in the exit plane [9, 10] and comparable to other in-chamber measurements [8].

III. Results

All experiments were performed on the Air Force Research Laboratory RDRE test rig located at Edwards Air Force Base in Edwards, CA. Measurements were made using gaseous CH_4 and O_2 as propellants over mass flow rates of 0.2–0.8 lbm/s and equivalence ratios of 0.8–1.7 . The $\dot{m} = 0.6$ lbm/s and $\phi = 1.1$ case serves as the baseline test case for which the key steps illustrating the conversion from raw laser intensity to intra-cycle ensemble thermochemical properties are shown. After detailing the method through which intra-cycle ensemble profiles are calculated, a higher flow rate test ($\dot{m} = 0.8$ lbm/s) and a higher equivalence ratio test ($\phi = 1.1$) are compared to the baseline test.

For each test, 500 ms of raw intensity data was recorded, consisting of 10 ms before ignition, 100 ms of startup transient, and up to 390 ms of steady state data. Test duration was limited by the maximum memory available on the data acquisition system. 50 ms of data recorded immediately before ignition was required to be used as the background I_0 signal intensity. The recording length of the test was deemed sufficient to capture quasi-steady state operation. Moreover, it should be noted that in some cases, particularly at the higher flowrates, the data acquisition system did not limit test time for flow since the sapphire window often cracked before 500 ms. Test conditions were repeated until >50 ms of quasi-steady state data was obtained, which yielded several hundreds to thousands of detonation cycles for a given test condition over which statistical analysis could be performed.

Taking the ratio of the background intensity I_0 to the measured attenuated signal during the test I_t and utilizing Eq. 1 gives the spectrally resolved absorbance shown in the left subplot of Fig. 2. Properties of individual lines are extracted

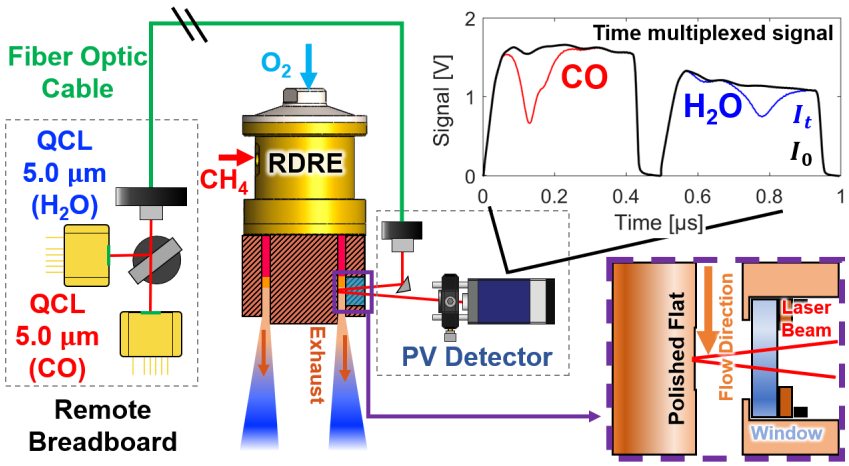

Fig. 1 Two-laser multiplexing setup on remote optical breadboard (left). Light is delivered via a fiber optic cable to the annulus of an RDRE (middle), where light is reflected off a polished flat on the center body, back towards a PV detector (right) which resolve transmitted intensity of the laser output signals (top right).

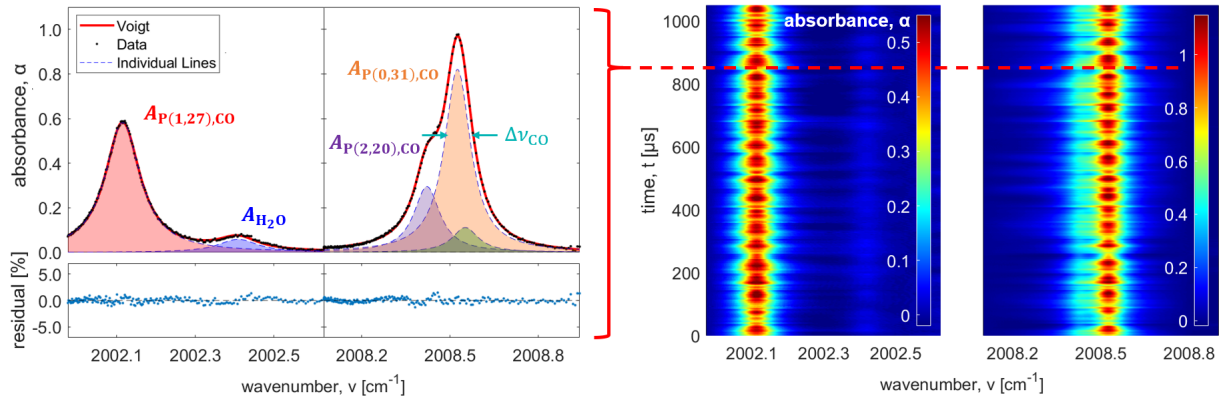

Fig. 2 (Left) Sample absorbance spectra at one time for the H_2O laser and CO laser. The individual line shapes determined through fitting the spectra are shown underneath the measured absorbance. (Right) Time evolution of spectrally-resolved absorbance for the H_2O laser and CO laser

through a least squares minimization of the residual between the measured spectra and the sum of Voigt profiles [25] approximating the shape of each line. A third line, P(3,14) (shown in green in Fig. 2), is present near the larger two CO features (P(0,31) and P(2,20)). This line is simulated by fixing its line position in the fit along with the ratio of linestrengths between the P(3,14) and P(0,31) lines. The line position, area, and collision width of the Voigt profile are floated along with a simple linear baseline correction utilized to account for distortion of the measured light intensity from mechanical vibrations and emission.

Certain optical components (dichroic mirrors, fiber couplings and spectral-bandpass filters) have wavelength-dependent transmission and reflection curves that change based on the angle of the incident light. While this is not a problem in the lab environment, harsh vibrations during engine firing can affect these components and cause distortion to the baseline laser intensity. Broadband emission from the combustion gas can also be received on the detector, artificially raising the measured light intensity. Both of these effects can not be completely eliminated but are significantly reduced by thoroughly securing components, centering the beam on all optics, and utilizing spectral-bandpass filters. A key benefit of the MHz scanned direct absorption technique used is that these effects appear frozen on the time scale of an individual scan. Offsetting and scaling the background I_0 on a scan-by-scan basis as part of the fitting routine corrects for these effects to mitigate their influence on the measured properties.

Figure 2 shows the results of this fitting routine with the linear baseline subtracted from the data and fit. Absorbance

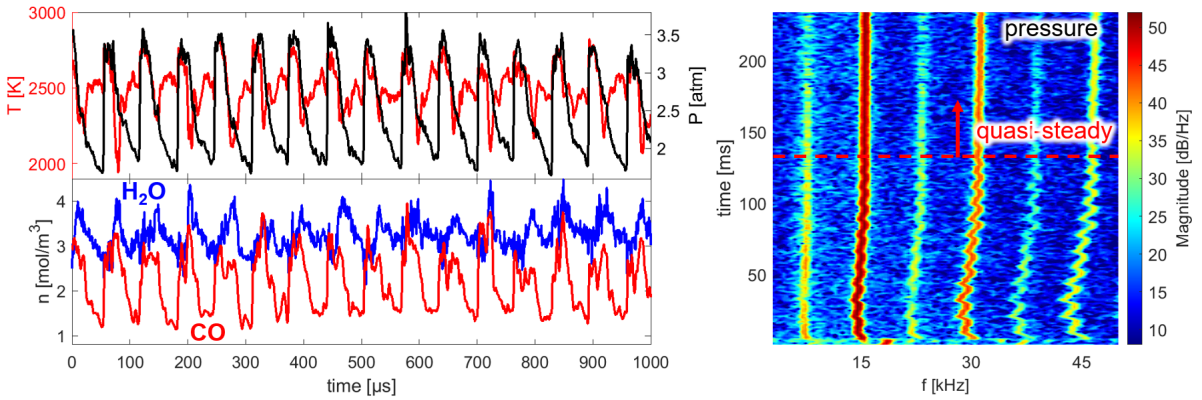

Fig. 3 Time-resolved thermophysical properties (left) and short-time Fourier transform of time resolved pressure. Above the red dashed line the test is considered quasi-steady state and intra-cycle ensemble profiles are taken (right).

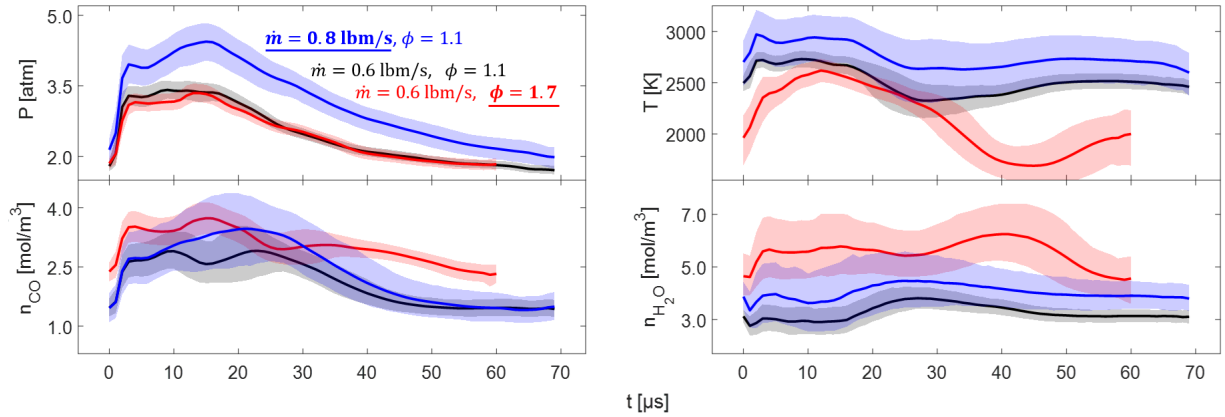

Fig. 4 Intra-cycle ensemble pressure (top left), temperature (top right) and species number density (bottom). Solid lines indicate cycle averages and the colored region represents the range of values from the 10th to 90th percentile.

for each scan is calculated as shown in Fig. 2. Applying this fitting procedure to each scan on the right subplot of Fig. 2 gives line areas and widths as a function of time which can be converted to thermophysical properties following the method outlined in Section II. The resulting time-resolved thermophysical properties are shown in the left of Fig. 3.

The pressure trace in Fig. 3 shows a clear structure of a sharp pressure increase across the oblique shock wave followed by an expansion. A cyclic pattern can be observed within the time-resolved data but there is significant variation in the shape and duration of each cycle. Time-resolved temperature and number density data show cyclic behavior of a similar frequency, albeit not as well-defined as the pressure data. In addition to time-resolved data, it is useful to calculate the average of all cycles referred to as intra-cycle ensemble profiles, and the pressure data trace is key to cycle indexing and subsequent statistical analysis.

The procedure for determining the intra-cycle ensemble profiles is given in [10] but the main steps are summarized here. First, a short-time Fourier transform (STFT) is performed on the pressure data as shown in the right of Fig. 3. The dominant frequency in the power spectrum is situated near 15 kHz, corresponding to the approximate cycle frequency observed in the time-resolved results. Each cycle is found by searching for the sharp increase in pressure observed across the oblique shock, i.e. by locating the local maxima of $\Delta P/\Delta t$ within the period of time determined by the peak frequency of the STFT. By identifying the bounds of individual cycles, we can take an average over all cycles within the steady-state portion of the test to construct the intra-cycle ensemble profiles. Figure 4 shows the intra-cycle ensemble pressure, temperature, and species number density for three MVP test cases of $\dot{m}$ = 0.6 lbm/s & ϕ = 1.1, $\dot{m}$ = 0.6 lbm/s & ϕ = 1.7 and $\dot{m}$ = 0.8 lbm/s & ϕ = 1.1 referred to as the baseline case, fuel-rich case, and high flow

rate case, respectively.

The pressure and temperature consistently show a sharp increase across the oblique shock followed by ~15 μs of relatively minimal change. Beyond this time, both the temperature and pressure begin to drop as the gas expands. The high flow rate test has an average pressure peak of 4.5 atm while the baseline and fuel-rich cases peak at 3.4 atm, with the fuel-rich case being ~0.2 atm lower in pressure between 3-11 μs. Temperature data for the high flow rate and baseline case trend closely to one another, though the high flow rate case exhibits temperatures elevated ~200 K above those seen for the baseline. The fuel-rich case demonstrates the greatest range of temperature oscillation, peaking at 2600 K and dropping as low as 1700 K; comparatively, the other two cases have a 400 K difference between their average peak and lowest point values. A possible explanation for this distinctive trend stems from injector dynamics causing a locally fuel-rich region behind the contact surface [10]. For the number density of both species, we observe a slight jump at the beginning of the cycle with this jump being more pronounced in the CO data.

The lightly-shaded regions bounding the ensemble averaged data represent the 10th and 90th percentile of oscillations measured over the quasi-steady state test duration. It should be noted that these oscillations are related to the physical changes or variance observed across cycles and are distinct from measurement uncertainty or error. A rigorous uncertainty analysis is pending for these particular test conditions, but the same CO line selection has been utilized previously with uncertainties found to be approximately 5%, 8% and 7% for T, P and n_{CO}, respectively, for RDRE exit plane data. Variance and uncertainty for n_{H_2O} is larger relative to n_{CO} due in part to relatively low absorbance and large uncertainty in the spectroscopic parameters (the HITRAN database lists the linestrength uncertainty as between 10-20% for the targeted H_2O line, which likely dominates the measurement uncertainty).

IV. Summary and Future Work

A mid-infrared laser absorption sensing strategy for simultaneous measurements of CO, H_2O, pressure, and temperature at MHz rates has been developed and employed for application to rotation detonation rocket engine studies. Measurements were performed inside the annulus of a methane-oxygen RDRE providing data at elevated pressures of 2–5 atm for a variety of mass flow rates and equivalence ratios. Time-resolved thermophysical properties provided insight into the cycle-to-cycle variation of a nominal test condition while intra-cycle mean properties were extracted to facilitate a direct comparison between test conditions. Future work is aimed at improving the quantification and reduction of uncertainties in these results.

Acknowledgements

This work was supported by the Air Force Research Laboratory (AFRL) and OptoKnowledge Systems Inc. under a Small Business Technology Transfer (STTR) program, Award No. FA864920C0326 with Dr. John W. Bennewitz as contract monitor, and Dr. Jason Kriesel as collaborator. Supplementary support was provided by the U.S. National Science Foundation (NSF), Award No. 1752516 and the Air Force Office of Scientific Research (AFOSR) Young Investigator Program (YIP) Award No. FA9550-19-1-0062 with Dr. Chiping Li as Program Officer. The authors would also like to thank Isaiah Jaramillo for assistance in running RDRE tests, Ilya Dunayevskiy for assistance in procuring hardware and Isabelle Sanders for aiding in the review of the final manuscript.

References

[1] Hargus, W. A., Schumaker, S. A., Paulson, E. J., and Danczyk, S. A., "Air Force Research Laboratory Rotating Detonation Rocket Engine Development," *2018 Joint Propulsion Conference*, American Institute of Aeronautics and Astronautics, Reston, Virginia, 2018. https://doi.org/10.2514/6.2018-4876, URL https://arc.aiaa.org/doi/10.2514/6.2018-4876.

[2] Lu, F. K., and Braun, E. M., "Rotating Detonation Wave Propulsion: Experimental Challenges, Modeling, and Engine Concepts," *Journal of Propulsion and Power*, Vol. 30, No. 5, 2014, pp. 1125–1142. https://doi.org/10.2514/1.b34802.

[3] Peng, W. Y., Cassady, S. J., Strand, C. L., Goldenstein, C. S., Spearrin, R. M., Brophy, C. M., Jeffries, J. B., and Hanson, R. K., "Single-ended mid-infrared laser-absorption sensor for time-resolved measurements of water concentration and temperature within the annulus of a rotating detonation engine," *Proceedings of the Combustion Institute*, Vol. 37, No. 2, 2019, pp. 1435–1443. https://doi.org/10.1016/j.proci.2018.05.021.

[4] Goldenstein, C. S., Spearrin, R. M., Jeffries, J. B., and Hanson, R. K., "Infrared laser absorption sensors for multiple performance parameters in a detonation combustor," *Proceedings of the Combustion Institute*, Vol. 35, No. 3, 2015, pp. 3739–3747. https://doi.org/10.1016/j.proci.2014.05.027.

[5] Spearrin, R. M., Goldenstein, C. S., Jeffries, J. B., and Hanson, R. K., "Quantum cascade laser absorption sensor for carbon monoxide in high-pressure gases using wavelength modulation spectroscopy," *Applied Optics*, Vol. 53, No. 9, 2014, p. 1938. https://doi.org/10.1364/AO.53.001938.

[6] Sanders, S. T., Baldwin, J. A., Jenkins, T. P., Baer, D. S., and Hanson, R. K., "Diode-laser sensor for monitoring multiple combustion parameters in pulse detonation engines," *Proceedings of the Combustion Institute*, Vol. 28, No. 1, 2000, pp. 587–594. https://doi.org/10.1016/s0082-0784(00)80258-1.

[7] Caswell, A. W., Roy, S., An, X., Sanders, S. T., Schauer, F. R., and Gord, J. R., "Measurements of multiple gas parameters in a pulsed-detonation combustor using timedivision-multiplexed Fourier-domain mode-locked lasers," *Applied Optics*, Vol. 52, No. 12, 2013, pp. 2893–2904. https://doi.org/10.1364/AO.52.002893.

[8] Mathews, G. C., Blaisdell, M. G., Lemcherfi, A. I., Slabaugh, C. D., and Goldenstein, C. S., "High-bandwidth absorption-spectroscopy measurements of temperature, pressure, CO, and H 2 O in the annulus of a rotating detonation rocket engine," *Applied Physics B: Lasers and Optics*, Vol. 127, No. 12, 2021, pp. 1–23. https://doi.org/10.1007/s00340-021-07703-9, URL https://doi.org/10.1007/s00340-021-07703-9.

[9] Nair, A., Lee, D., Pineda, D., Kriesel, J., Hargus, W., Bennewitz, J., Danczyk, S., and Spearrin, R., "MHz laser absorption spectroscopy via diplexed RF modulation for pressure, temperature, and species in rotating detonation rocket flows," *Applied Physics B*, Vol. 126, No. 8, 2020, p. 138. https://doi.org/10.1007/s00340-020-07483-8, URL https://link.springer.com/10.1007/s00340-020-07483-8.

[10] Nair, A. P., Lee, D. D., Pineda, D. I., Kriesel, J., Hargus, W. A., Bennewitz, J. W., Bigler, B., Danczyk, S. A., and Spearrin, R. M., "Methane-Oxygen Rotating Detonation Exhaust Thermodynamics with Variable Mixing, Equivalence Ratio, and Mass Flux," *Aerospace Science and Technology*, Vol. 113, 2021, p. 106683. https://doi.org/10.1016/j.ast.2021.106683.

[11] Strakey, P. A., and Ferguson, D. H., "Validation of a Computational Fluid Dynamics Model of a Methane-Oxygen Rotating Detonation Engine," *AIAA Science and Technology Forum and Exposition, AIAA SciTech Forum 2022*, 2022. https://doi.org/10.2514/6.2022-1113.

[12] Goldenstein, C., Spearrin, R., Jeffries, J., and Hanson, R., "Infrared laser-absorption sensing for combustion gases," *Progress in Energy and Combustion Science*, Vol. 60, 2017, pp. 132–176. https://doi.org/10.1016/j.pecs.2016.12.002, URL https://linkinghub.elsevier.com/retrieve/pii/S0360128516300843.

[13] Lee, D. D., Bendana, F. A., and Spearrin, R. M., "Laser Absorption Spectroscopy of Carbon Monoxide near 4.97 μm for Temperature and Species Measurements in Hydrocarbon-Fueled Rockets," *2018 AIAA Aerospace Sciences Meeting*, American Institute of Aeronautics and Astronautics, 2018. https://doi.org/10.2514/6.2018-1778.

[14] Pineda, D. I., Bendana, F. A., Schwarm, K. K., and Spearrin, R. M., "Multi-isotopologue laser absorption spectroscopy of carbon monoxide for high-temperature chemical kinetic studies of fuel mixtures," *Combustion and Flame*, Vol. 207, 2019, pp. 379–390. https://doi.org/10.1016/j.combustflame.2019.05.030, URL https://linkinghub.elsevier.com/retrieve/pii/S0010218019302433.

[15] Rothman, L., Gordon, I., Barber, R., Dothe, H., Gamache, R., Goldman, A., Perevalov, V., Tashkun, S., and Tennyson, J., "HITEMP, the High-Temperature Molecular Spectroscopic Database," *Journal of Quantitative Spectroscopy and Radiative Transfer*, Vol. 111, No. 15, 2010, pp. 2139–2150. https://doi.org/10.1016/j.jqsrt.2010.05.001.

[16] Hanson, R., Spearrin, R., and Goldenstein, C., *Spectroscopy and Optical Diagnostics for Gases*, Springer International Publishing, 2016. https://doi.org/10.1007/978-3-319-23252-2.

[17] Minesi, N. Q., Richmond, M. O., Jelloian, C. C., Kuenning, N. M., Nair, A. P., and Spearrin, R. M., "Multi-line Boltzmann regression for near-electronvolt temperature and CO sensing via MHz-rate infrared laser absorption spectroscopy," *Applied Physics B: Lasers and Optics*, Vol. 128, No. 12, 2022, p. 214. https://doi.org/10.1007/s00340-022-07931-7, URL https://link.springer.com/10.1007/s00340-022-07931-7.

[18] Gordon, I., Rothman, L., Hargreaves, R., Hashemi, R., Karlovets, E., Skinner, F., Conway, E., Hill, C., Kochanov, R., Tan, Y., Wcisło, P., Finenko, A., Nelson, K., Bernath, P., Birk, M., Boudon, V., Campargue, A., Chance, K., Coustenis, A., Drouin, B., Flaud, J., Gamache, R., Hodges, J., Jacquemart, D., Mlawer, E., Nikitin, A., Perevalov, V., Rotger, M., Tennyson, J., Toon, G., Tran, H., Tyuterev, V., Adkins, E., Baker, A., Barbe, A., Canè, E., Császár, A., Dudaryonok, A., Egorov, O., Fleisher, A., Fleurbaey, H., Foltynowicz, A., Furtenbacher, T., Harrison, J., Hartmann, J., Horneman, V., Huang, X., Karman, T., Karns, J., Kassi, S., Kleiner, I., Kofman, V., Kwabia–Tchana, F., Lavrentieva, N., Lee, T., Long, D., Lukashevskaya, A., Lyulin, O., Makhnev, V., Matt, W., Massie, S., Melosso, M., Mikhailenko, S., Mondelain, D., Müller, H., Naumenko, O., Perrin, A., Polyansky, O., Raddaoui, E., Raston, P., Reed, Z., Rey, M., Richard, C., Tóbiás, R., Sadiek, I., Schwenke, D., Starikova, E., Sung, K., Tamassia, F., Tashkun, S., Vander Auwera, J., Vasilenko, I., Vigasin, A., Villanueva, G., Vispoel, B., Wagner, G., Yachmenev, A., and Yurchenko, S., "The HITRAN2020 molecular spectroscopic database," *Journal of Quantitative Spectroscopy and Radiative Transfer*, Vol. 277, 2022, p. 107949. https://doi.org/10.1016/j.jqsrt.2021.107949.

[19] Gamache, R. R., Vispoel, B., Rey, M., Nikitin, A., Tyuterev, V., Egorov, O., Gordon, I. E., and Boudon, V., "Total internal partition sums for the HITRAN2020 database," *Journal of Quantitative Spectroscopy and Radiative Transfer*, Vol. 271, 2021, p. 107713. https://doi.org/10.1016/j.jqsrt.2021.107713, URL https://doi.org/10.1016/j.jqsrt.2021.107713https://linkinghub.elsevier.com/retrieve/pii/S0022407321002065.

[20] Nair, A. P., Minesi, N. Q., Kuenning, N. M., Keller, A. R., and Mitchell Spearrin, R., "Optical pressure sensing at MHz rates via collisional line broadening of carbon monoxide: uncertainty quantification in reacting flows," *(submitted)*, ????

[21] Smith, G. P., Golden, D. M., Frenklach, M., Moriarty, N. W., Eiteneer, B., Goldenberg, M., Bowman, C. T., Hanson, R. K., Song, S., Gardiner, W. C., Lissianski, V. V., and Qin, Z., "GRI-MECH 3.0," , 1999. URL http://combustion.berkeley.edu/gri-mech/version30/text30.html.

[22] Browne, S., Ziegler, J., and Shepherd, J. E., "Numerical Solution Methods for Shock and Detonation Jump Conditions," *GALCIT Report FM2006.006*, 2004.

[23] Goodwin, D. G., Moffat, H. K., and Speth, R. L., "Cantera: An object-oriented software toolkit for chemical kinetics, thermodynamics, and transport processes," , 2018. https://doi.org/10.5281/zenodo.170284.

[24] Nair, A. P., Minesi, N. Q., Jelloian, C., Kuenning, N. M., and Spearrin, R. M., "Extended tuning of distributed-feedback lasers in a bias-tee circuit via waveform optimization for MHz-rate absorption spectroscopy," *Measurement Science and Technology*, Vol. 33, No. 10, 2022, p. 105104. https://doi.org/10.1088/1361-6501/ac7b13, URL https://iopscience.iop.org/article/10.1088/1361-6501/ac7b13.

[25] McLean, A., Mitchell, C., and Swanston, D., "Implementation of an efficient analytical approximation to the Voigt function for photoemission lineshape analysis," *Journal of Electron Spectroscopy and Related Phenomena*, Vol. 69, No. 2, 1994, pp. 125–132. https://doi.org/10.1016/0368-2048(94)02189-7.